ISSN (Print) : 0974-6846
Indian Journal of Science and Technology, Vol 8(26), DOI: 10.17485/ijst/2015/v8i326/80679, October 2015 ISSN (Online) : 0974-5645

Impact Properties of Laminating Type in EVA and CFRP

Hong-Gun Kim[1], Hee-Jae Shin[2], Min-Sang Lee[2] and Lee-Ku Kwac[1*]

[1]Department of Mechanical and Automotive Engineering, Jeonju University, Republic of Korea; kwac29@jj.ac.kr
[2]Department of Mechanical Engineering, Jeonju University, Republic of Korea

Abstract

This study deals with Carbon Fiber Reinforced Plastic (CFRP), which is receiving much attention in various fields because of its excellent properties such as high specific strength, specific stiffness, and corrosion resistance. Since CFRP is vulnerable to impact damage owing to its brittle nature, this study intends to overcome this vulnerability by using Ethylene Vinyl Acetate (EVA), which possesses excellent cracking resistance and flexibility. In this study, impact tests were conducted by fabricating test specimens through various lamination methods using the impact theory. In addition, the size, shape, and tendency of a defect in impact-tested specimens were identified using an IR thermal imaging camera through the thermal imaging theory.

Keywords: Carbon Fiber Reinforced Plastic, Ethylene Vinyl Acetate, Impact Test, Lamination, Thermoelastic

1. Introduction

Since a CFRP composite has excellent mechanical properties such as high specific strength, specific stiffness, and corrosion resistance, in addition to having the advantage of reducing the mass by 20%–50% compared to that in the case of using a metallic alloy, it is being used more frequently in various fields, e.g., in the aerospace industry, including in centrifuge rotators, compressor moving blades of a plane, and rotary wings in a helicopter. However, the most serious drawback of the application of a CFRP laminate is its vulnerability to impact, and impact damages caused by several types of impacting bodies, such as small stones or fractures, are unavoidable when the laminate is used in a plane or as other structural members[1,2].

In the actual use of a CFRP laminate in a structure, the risk of destruction by an impact load should be thoroughly considered in order to prevent the occurrence of any destruction beforehand. However, the reliability of CFRP is presently secured by experimental methods because no method has yet been established for quantitatively identifying which damage proceeds in which destruction mode[3].

Therefore, this study performs experiments in accordance with the specifications and methods specified in ASTM D7136 standards in order to establish the relationship between the amount of impact energy and the damage of a CFRP laminate via defect detection based on the thermal imaging theory for different lamination methods of CFRP and an EVA sheet, which possesses excellent crack resistance flexibility against CFRP[4].

2. Theoretical Background

2.1 Chemical Theoretical Background

Figure 1 shows the bonding property between epoxy and EVA, both of which were added to the CFRP. The carboxyl in EVA reacts with the epoxy reactor to cause dehydration, which leads to physical and chemical bonding among EVA, the prepreg, and epoxy.

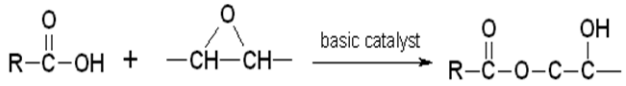

Figure 1. Reaction of a carboxyl group with an epoxy.

* Author for correspondence

2.2 Impact Test Theory

Impact[5] test method determines the damage resistance of multidirectional polymer matrix composite laminated plates subjected to drop-weight impact event. The composite material forms are limited to continuous-fiber reinforced polymer matrix composites, with the range of acceptable test laminates and thicknesses defined in ASTM D7136. The damage resistance properties generated by this test method arc highly dependent upon several factors, which include specimen geometry, layup, impact geometry, impact mass, impact force, impact energy, and boundary conditions. Thus, results are generally not scalable to other configurations and are particular to the combination of geometric and physical conditions tested.

The impact energy and absorbed energy can be determined from the drop-weight test in the following test conditions. Equation (1) shows the equation for determining the impact energy.

(1)

(= Impact Energy, m = weight of impact, = velocity of impact)

Equation (2) shows the equation for determining the absorbed energy.

(2)

(=absorbed energy by time[j], g=9.81 m, δ = impactor displacement by time)

2.3 Thermographic Theory

Figure 2 shows the principle of the infrared camera.

The IR thermal imaging camera[6] does not capture the object itself, but rather detects the energy of the IR wavelength form, which is a kind of electronic wave radiated from the surface of the object, and it measures the strength of the surface radiant heat of the object and then represents the strength through different colors. Furthermore, it is able to detect a defect by providing a heat source to the defect area, as shown in Figure 3[7].

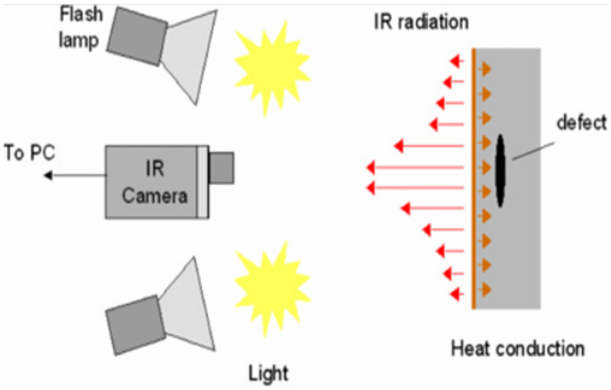

Figure 3. Fault detection method using an infrared thermal imaging camera.

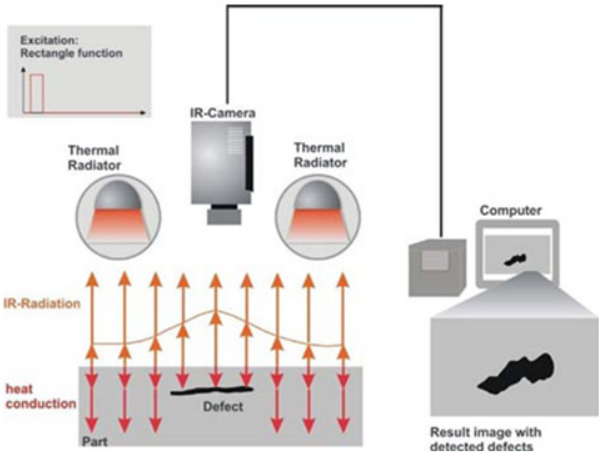

Figure 4. The principle of transient thermography.

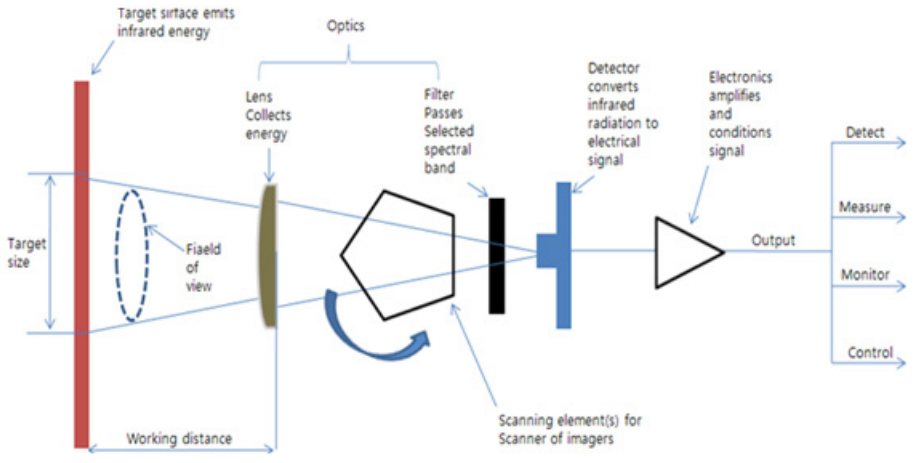

Figure 2. Principles of infrared thermal imaging camera.

The material to be inspected by transient thermography is heated by a high performance heat source. Figure 4 shows that the heat penetrates into the material from the surface in a form of one-dimensional thermal conduction in the beginning stage. When such heat wave front reaches a defect, conductions are interrupted, the heat scatters around the defect in a form of two-dimensional conductions; such affects the surface temperature; the defect acts as an internal heat source, and causes variations depending on the duration of the temperature different from positions without defects. When the heat wave passes the defect, it recovers the form of one-dimensional conduction[8].

In the measurement, it is important to measure the moment when the two-dimensional thermal conduction appears, and such is, in particular, important in the materials with higher thermal conduction characteristics. Therefore, in shorter duration of heating time, it uses normally a high-performance infrared thermographic camera with higher frame rate. Figure 5 shows a temperature profile that appears when the materials is heated momentarily, in which A is confirmed to be the temperature profile appeared at the part without defects and B at the part with defects[9,10].

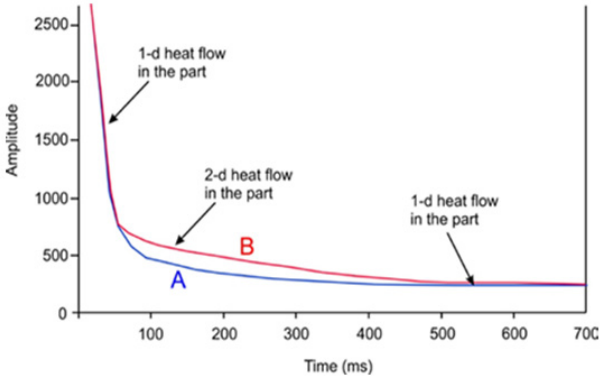

Figure 5. Typical temperature profile in instantaneous heating.

The first step for the assessment is establishing an assumption the temperature profiles measured at each pixel of an image with proper analytical functions (the answers of the thermal conduction differential equation which are solved by polynomial expressions). The additional assessments on such analytical functions have important merits in rapid reduction of data volume, removal of noises from measurement signals, etc[8].

2.4 Thermal Conduction Theory

This method rests on the well-known one-dimensional thermal conduction equation.

$$\frac{\partial^2 T(x,t)}{\partial x^2} = \frac{1}{\alpha}\frac{\partial T(x,t)}{\partial t} \tag{3}$$

If the answer of the surface in a half-infinite quantity were calculated from the aforementioned equation (x = 0).

$$T_{s-i}(0,t) = \frac{Q/\rho c}{\sqrt{\pi \alpha t}} \tag{4}$$

Where, Q (j/m^2) refers to the strength of the input energy, ρ to the density, c to the thermal capacity, α to the thermal diffusivity, respectively. If λ were imported into the Equation (4) and simplified, the Equation (5) is obtained. Where, e stands for the thermal effusively.

$$T = \frac{Q}{\sqrt[e]{\pi t}} with\ e = \sqrt{\lambda \rho c} \tag{5}$$

Assuming that it is one-dimensional conduction, the thermal diffusion on the side surface is disregarded until it reaches the boundary surface of the internal defect where the aforementioned abnormal part exists. Therefore, in the Pursed Thermography (PT) with a shorter cycle, the one-dimensional thermal conduction equation is the answer of the Equation (6) in a half-infinite quantity, and the Equation (7) which shows a linear form in the algebra area represents the facts as described in the following.

$$InT = 1n\left(\frac{Q}{\sqrt[e]{\pi}}\right) - \frac{1}{2}lnt \tag{6}$$

The Equation (7) presents a slop of -0.5 in the specimen in a half-infinite quantity. The linear form is broken when it contacts the front or side surfaces. The input energy (Q) and the material variable (e) of the specimen contain an obstacle clause, and the behavior of the linear form remains unchanged even if the experimental condition were changed. The linear from appears independent from the PT image points. Therefore, the defected regions and the normal regions are identifiable.

Actually, the ideal linear behavior in the algebra area is affected by many uncertain factors. However, the method obtaining logarithms that softens the curve is changeable so as to describe such behavior in higher precision. An example of the functions of the Equation (8) is a low-dimensional polynomial interpolation which can describe easily the log value of the time at the point close to the reality.

$$\ln[T(t)]=\alpha_0+\alpha_1 1n(t)+\alpha_2[1n(t)]^2+\ldots+\alpha_n[1n(t)]^n \quad (7)$$

The additional merit of such developments lies on the possibility to obtain the necessary thermal signals selectively. If each point was once converted in accordance with the Equation (7), the original data can be converted using the Equation (8).

$$[T(t)]=\exp\alpha_0+\alpha_1 1n(t)+\alpha_2[1n(t)]^2+\ldots+\alpha_n[1n(t)]^n \quad (8)$$

Thus, the temperatures-times corresponding to each point in the initial linear area are saved. The matrix converted to all elements can be easily converted to the image sequence with any length at the desired time interval and frequency.

3. Specimen Production and Test Methods

3.1 Properties and Molding Conditions CFRP

In this study, specimens for the impact tests were fabricated by cross-laminating the lightweight CFRP with the EVA sheets, which have excellent impact resistance, in order to overcome the vulnerability of CFRP to impact. The material properties of the CFRP used in the specimen are listed in Table 1.

Table 1. Physical properties of CFRP

Thickness [mm]	Fiber Areal Wt $\frac{g}{[m^2]}$	Resin Content [%]	Total Wt $\frac{g}{[m^2]}$
0.227	240	41	336
Tensile Strength $\frac{kgf}{[mm^2]}$	TensileModulus $\frac{kgf}{[mm^2]}$	Fiber Density $\frac{g}{[m^2]}$	Resin Density $\frac{g}{[m^2]}$
450	24×10^3	1.77	1.2

3.2 Specimen Size and Laminated Methods[1,11]

As shown in Figure 6, the specimens were fabricated by four different lamination methods, and specimen 4.5T was used a reference. The four lamination methods were applied under the same conditions: pressure of 100 kg/cm^2, CFRP stiffening temperature of 125°C, and molding time of 90 min. The same specimens as those shown in Figure 7 were fabricated by the hot-press molding method.

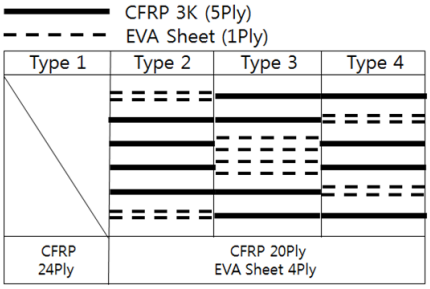

Figure 6. Laminated form according to the test specimen.

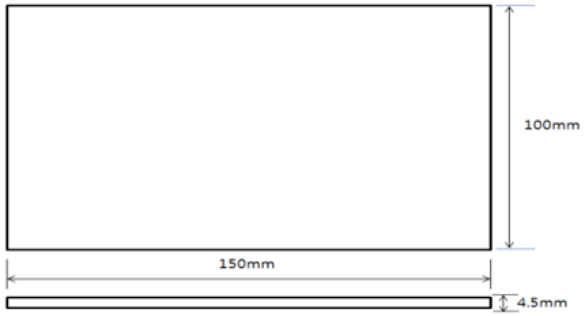

Figure 7. Impact specimen diagram.

3.3 Impact Test Method

Hammer-drop tests[1,11] were performed in accordance with ASTM D7136 specifications. Figure 8 shows the impact test that was performed using the hammer-drop tester Dynatup 9250HV (Instron Corporation). Table 2 presents the test conditions.

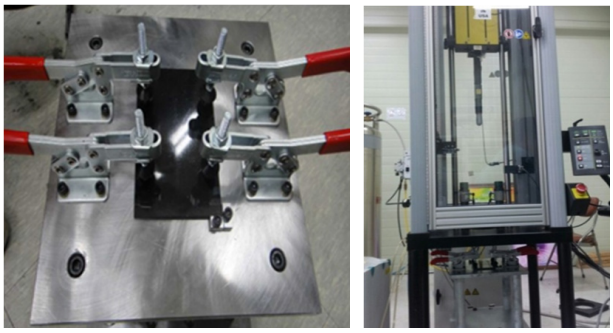

Figure 8. Impact device with cylindrical tube impacotr guide mechanism.

Table 2. Experiment condition for drop-weight impact test

Impact velocity [m/s]	Drop Weight [kg]	Impact Energy [J]
3.6358	6.1012	40.3261

3.4 Thermal Imaging Shooting Techniques using Transient

Thermal imaging[12,13] was used to shoot 2.5kW × 2EA halogen lamps. Also prepare a test piece by the black body target emissivity close to 1. And it was taken using the transient technique.

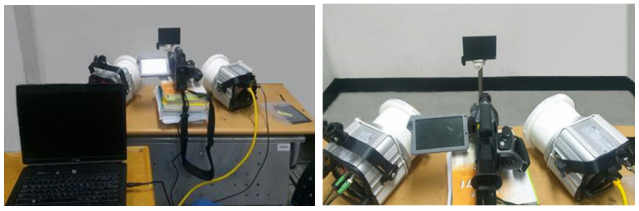

Figure 9. Thermal image taken using a halogen lamp.en.

4. Results and Discussion

4.1 Impact Test Results

The impact tests were performed according to the type of lamination of the EVA sheet, and as shown in Table 3, the strain rate versus load for the different types of laminations and the absorption energy depending on the impact energy were verified and compared in Figure 10 in graphs. Table 3 summarizes the experimental data.

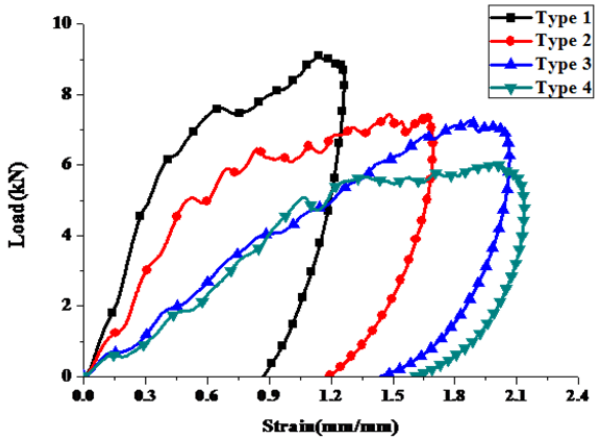

Figure 10. Load-Strain curve.

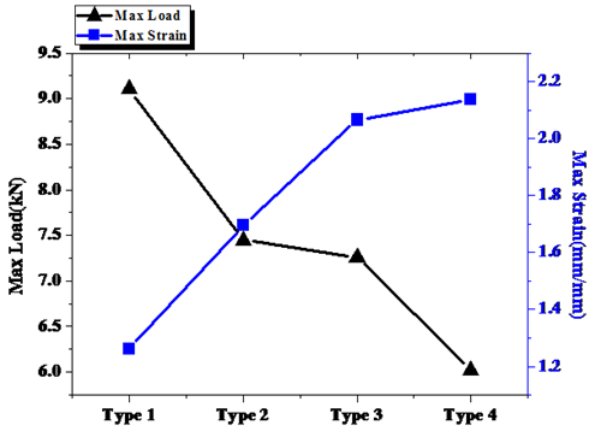

Figure 11. Max load-Max strain curve.

When the almost constant impact energy was applied to Type 1 - Type 4 specimens, compared with Type 1 specimen, the absorbed energy decreased by 1.4% in Type 2 and Type 3 specimens, and by 5.6% in Type 4 specimen. Figure 11 is a graph comparing the load and deformation data for each type.

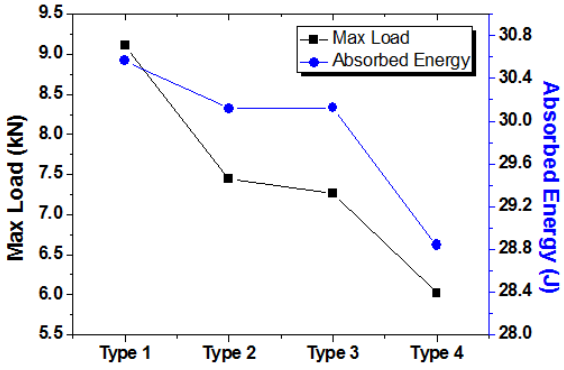

Figure 12. Max load-Asorbed energy curve.

The maximum loads of the Type 2, Type 3, and Type 4 specimens reduced by about 18.19%, 20.00%, and 33.91%, respectively, compared to that of the Type 1 specimen, and the maximum strains of the Type 2, Type 3, and Type 4 specimens increased by about 34.29%, 63.67%, and 69.38%, respectively.

Table 3. Impact test results data

Specimen	Impact Velocity [m/s]	Impact Energy [J]	Absorbed Energy [J]	Max Load [kN]	Max Strain [mm/mm]
Type 1	3.6310	40.2202	30.5627	9.105215	1.261919
Type 2	3.6399	40.4179	30.12009 (-1.448%)	7.448146 (-18.19%)	1.694681 (34.29%)
Type 3	3.6288	40.1700	30.12624 (-1.428%)	7.26163 (-20.20%)	2.065394 (63.67%)
Type 4	3.6313	40.2255	28.84014 (-5.636%)	6.017303 (-33.91%)	2.137242 (69.36%)

The absorption energies for the different lamination types were almost similar, but since the maximum loads decreased and the maximum strains increased as the type transitioned from Type 1 to Type 4, the impacts applied to the test specimens were similar, and it seemed that the breakage of the material would reduce because the cracking resistance and flexibility increased as the distribution of the EVA sheet became more uniform.

Figure 12 shows a comparison graph for the maximum loads and absorption energies for the different lamination types. The absorption energies for the different lamination types were almost similar, but since the maximum loads decreased and the maximum strains increased as the type transitioned from Type 1 to Type 4, the impacts applied to the test specimens were similar, and it seemed that the breakage of the material would reduce because the cracking resistance and flexibility increased as the distribution of the EVA sheet became more uniform.

4.2 Thermal Imaging Shooting Results

After subjecting a specimen to the impact test, the shape and size of defects in the specimen were detected by the IR thermal imaging camera, as shown in Figure 13.

From the detection results of the IR thermal imaging camera, it seemed that the Type 1 specimen showed severe damage because its front received most of the damage given that it was fabricated with only CFRP; this specimen did not show significant transfer of impact to its rear.

When the mixed lamination method of EVA was changed in the order of Type 2, Type 3, and Type 4, the front of the Type 4 specimen, in which the EVA sheet was evenly distributed, showed the least damage, similar to the damage observed in the rear. It is thought that the size of a defect decreases as the EVA sheet is more evenly mixed and laminated.

5. Conclusion

In this study, the specimens were fabricated by four lamination methods using CFRP and EVA. The specimens were tested using a hammer-drop tester, and additionally, an IR thermal imaging camera was used to determine the shapes and sizes of the defects in the specimens. The following are the findings obtained in the study.

- The absorption energy decreased as the mixed lamination of CFRP and EVA became more evenly distributed, and this decrease is thought to be caused by the increased resistance and flexibility.
- The absorption energy and maximum load showed only a slight difference between specimens of the

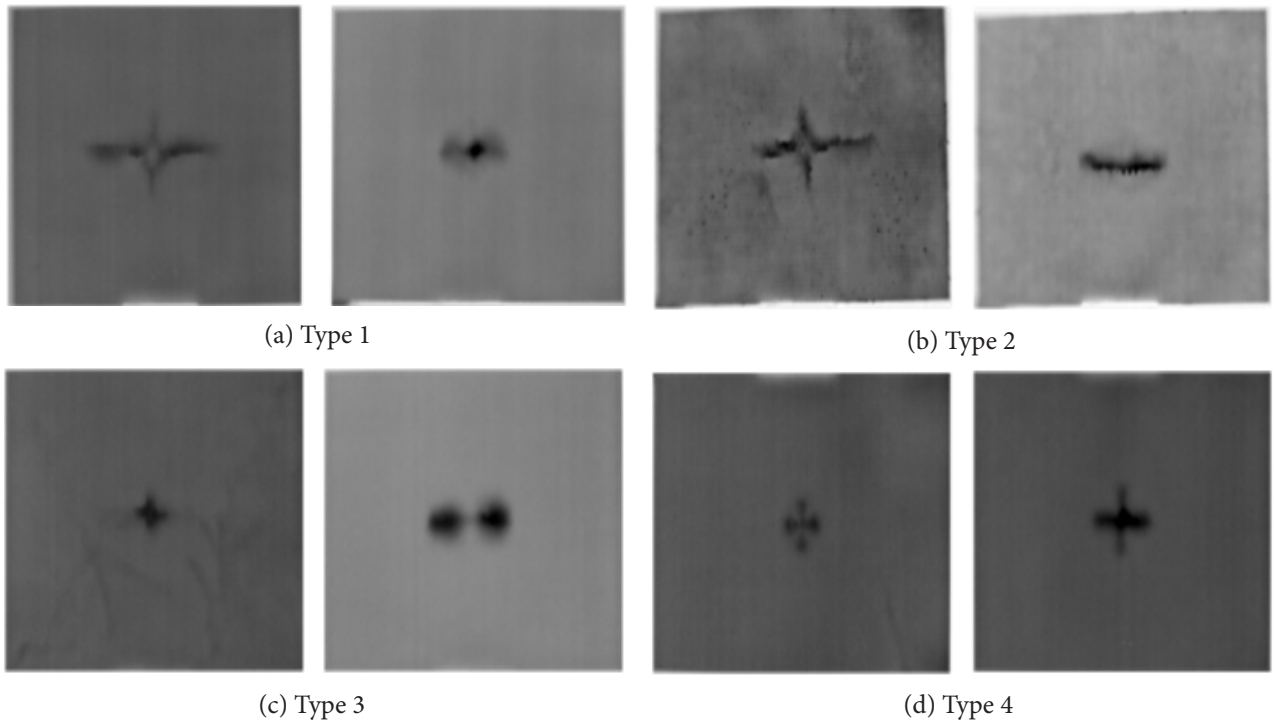

(a) Type 1 (b) Type 2

(c) Type 3 (d) Type 4

Figure 13. Fault detection results using a thermal imaging camera.

Type 2 and Type 3 lamination methods, but the strain rate in the Type 2 specimen was about 21.875% lower than that in the Type 3 specimen.

- The absorption energies for the different lamination types were almost similar, but since the maximum loads decreased and the maximum strains increased as the type transitioned from Type 1 to Type 4, the impacts applied to the test specimens were similar, and it seemed that the breakage of the material would reduce because the cracking resistance and flexibility increased as the distribution of the EVA sheet became more uniform.
- From the detection results of the IR thermal imaging camera, it was confirmed that the size of the defect decreased as the mixed lamination became more evenly distributed.
- It is thought that experiments performed with additional types of specimens apart from those used in this study will stimulate the use of the considered composite material.

6. Acknowledgement

This research was supported by the National Foundation of Korea (NRF) grant funded by the Korea Government (MISP) (No.2014R1A2A1A11054594) and (No.2014R1A2A1A11053533).

7. References

1. Lee MS, Shin HJ, Yonn HK, Kang KP, Kim TH, Kwac LK, Kim HG. A study on the impact properties of the structural forms of CFRP and EVA. KSMTE Annual Spring Conference. 2015. p. 125.
2. Im KH, Yang IY, Kim GH. Bending fatigue strength of CFRP composite lamination subjected to impact loading. Energy and Resouces Institute. 1995; 17(2):1–14.
3. Yang IY, Jung JA. A study on characteristics of impact fracture in CFRP laminate plates. Transactions of Korea Society of Automotive Engineers. 1995; 13(5):38–46.
4. Lee JH, Hong SC. Study on the controlled preparation of polyolefin based block or graft copolymers. Elastomers and Composties. 2013; 48(1):30–8.
5. Shin HJ, Ko SH, Kim JS, Kim YJ, Kim KE, Kwac LK, Kim HG. Analysis of mechanical and theramal properties according to laminated oreintation of CFRP composite through impact test. 9th International Conference on Fracture and Strength of Solids. 2013. p. 1–8.
6. Kim JS, Kim HG, Shin HJ, Ko SH, Kim YM, Cha YJ, Kwac LK. A study of detecting defect carbon-carbon composties by infrared thermogragphy. International Symposium on Green Manufacturing and Applications. 2011.
7. Shin HJ. The strength evaluation and nondestructive testing of carbon fiber composties study [Masters Degree]. Jeonju University. 2013. p. 30–8.
8. Junyan L, Qingju T, Yang W. The study of inspection on SiC coated carbon-carbon composite sith subsurface defects by lock-in thermography. Composites Science and Technology. 2012; 72:1240–50.
9. a la Faculte. Quantitative subsurface defect evaluation by pulsed phase thermography: Depth retieval with the phase [Philosophiae Doctor, PhD]. Genie Electrique Pour, Facultedes Sciences Et De Genie. Universitelaval Quevec. 2005.
10. Flir. No data. 2012 Dec 21. Available from: http://www.nondestructivetestingsolutions.com/htm/ir.htm
11. Standard test method for measuring the damage resistance of a fiber reinforce polymer matrix compostie to a drop-weigth impact event.
12. Avdelidis NP, Ibarra-Castanedo C, Theodorakeas P, Bendada A, Saarimaki E, Kauppinen T, Koui M, Maldague XPV. NDT characterisation of carbon-fiber and glass-fibre composties using non-invasive imaging techniques. International Conference on Quantitative Infrared Thermography.
13. Shin HJ, Kwac LK, Ko SH, Kim TH, Kim HG. A study on impact strength of CFRP using infrared thermography. Adv Mater Res. 2013; 628:390–5.